Comparative Study on Shear Wave Speed Estimation Algorithms in ARFI for Improving Its Reliability

Jinying Yang, Congzhi Wang, *IEEE Member*, Weibao Qiu, *IEEE Member*, Hairong Zheng, *IEEE Member*

***Abstract* — Quantitatively assessing the tissue stiffness with acoustic radiation force impulse (ARFI) method has proved its worth in clinical trials. Much attention has been focused on the research of the displacement estimation algorithm in ARFI. However, the subsequent shear wave speed estimation part can also affect the accuracy and reliability of the results. In this study, several algorithms for shear wave speed estimation were designed and compared using the ultrasound radio-frequency data collected from a self-developed ARFI system. These RT based algorithms were classified as two types: the transformation being performed on the time-location displacement matrix or on the time-depth displacement matrix. The algorithms in Type I attempt to find the best trajectory of the shear wave propagation in one depth, while those in Type II try to directly find the time points when the wavefront passed each lateral location in the whole depth range. Experiments were performed on soft tissue mimicking phantom and *ex vivo* pork tissue sample. The reliability of repeated measurements and the computation time of these algorithms were compared to find the most stable and time-saving one for ARFI. The results can give us inspiration on how to design a better algorithm for shear wave speed estimation and help to improve the measurement reliability of ARFI.**

I. Introduction

Acoustic radiation force impulse (ARFI) is a quantitative method for tissue stiffness assessment [1]. In ARFI, acoustic radiation force is generated by a focused ultrasound beam and induces localized small displacements in the soft tissue (generally the amplitude is only 1~10 μm) [2]. Subsequently shear wave arises and propagates away from this vibration source. Its propagation can be tracked by a high frame rate ultrasound scanner. Then the shear wave speed is evaluated in the region of interest (ROI) and converted to the Young's modulus [3]. ARFI has been used in the commercial systems developed by Siemens and Philips. It has been validated on many diseases and organs like liver, breast, thyroid, pancreas, etc., and has proved its worth in clinical trials [4].

Previous studies on ARFI algorithms mainly focused on the displacement estimation part. The key issue is to reduce the estimation errors caused by the decorrelation of the ultrasound radio-frequency (RF) signals and to speed up the calculation simultaneously [5-9]. However, the influence of these errors can be also compensated during the subsequent shear wave speed estimation part. The direct method for this is to solve the inverse problem of Helmholtz equation, which requires computing the second-order derivatives of the displacement signals to recovery the shear wave speed [10-13]. This method has been successfully applied in magnetic resonance elastography (MRE), but can only achieve limited success in ultrasound elastography because of the inherent noisy nature of the RF echo signals [14-16]. Another simple algorithm generally used in shear wave estimation is the time-of-flight (TOF) method, in which the shear wave propagation is characterized as a function of time. The travelling shear wave can be tracked at different lateral locations by cross-correlation or time-to-peak (TTP) methods and the shear wave speed can be calculated by dividing the distance by the travel time [17-21]. However, it also has limitations that some factors, such as physiological motion, low signal-to-noise ratio (SNR) displacement signals and spatial inhomogeneities in tissue, can all negatively affect the accuracy of the estimated shear wave speed, especially on the *in vivo* patients' data.

In a previous study, Rouze et al. used a RT (RT) based TOF method to improve the robustness of shear wave speed estimation in ARFI [22]. The displacement signals at one depth and four lateral tracking locations were formed as a time-location matrix. RT summed up the data along a straight-line trajectory in the matrix. The trajectory corresponding to the maximum summation value was the best approximation of the time sequence when the wavefront passed the four lateral locations. However, their method didn't provide a solution that how to determine the depth where the displacement signals would be selected. Generally the focal depth would be selected, but if some errors accidentally occurred on one of these four displacement signals, the estimated shear wave speed might be totally wrong. And if multiple depths were selected, how to select them and how to make a tradeoff between reliability and computation intensity would be another problem.

The aim of this study is to compare the results of several RT based algorithms of shear wave speed estimation using the real RF data collected from an self-developed ARFI system. The results can give us inspiration on how to design a better algorithm for shear wave speed estimation and help to improve the measurement reliability of ARFI.

II. Methods

The algorithms we used were classified into two types: one type was that the RT being performed on time-location displacement matrix, similar to that used in Rouze's study; another type was that the RT being performed on time-depth

Resrach supported by the National Natural Science Foundation of China (Grant No. 81027006, 61302038 and 61302039).

YJ. Yang, CZ. Wang, WB. Qiu and HR. Zheng are all with the Paul C. Lauterbur Research Center for Biomedical Imaging, Institute of Biomedical and Health Engineering, Shenzhen Institutes of Advanced Technology, Chinese Academy of Sciences, Shenzhen, China. (Corresponding author: CZ. Wang; phone: +86-755-86392264; fax: +86-755-86392299; e-mail: cz.wang@siat.ac.cn; the other authors' emails: jy.yang@siat.ac.cn; wb.qiu@siat.ac.cn; hr.zheng@siat.ac.cn).

displacement matrix, which attempted to directly find the time points when the wavefront passed each lateral location. Here they are introduced separately as follows.

A. Type I: RT on time-location displacement matrix

In these algorithms, displacement signals are expressed as a matrix of time t and lateral location n (n=1, 2, 3, 4). The distance between two adjacent locations is x. To improve the temporal resolution, a 20 times cubic spline interpolation was first performed on each row of data in the time direction. In this matrix, we can suppose a solution space of linear trajectories extend from a starting position (1, t_{start}) to an ending position (4, t_{end}), where $t_{start}<t_{end}$, and the relationship between distance and time can express as

$$x * 3 = (t_{end} - t_{start}) * v \quad (1)$$

where shear wave speed v can be calculated. Theoretically for each four displacement signals obtained at the same depth, we can get one shear wave speed value.

Considering the selected depth for the above calculation, Type I algorithms tested in our study can be sorted into three cases: (1) at a single focal depth, (2) at several artificially selected depths and (3) at all the depths. They are described in detail in the following sections.

(1) After tissue displacement estimation, four time-depth displacement matrixes were obtained, each corresponding to one lateral location. The first 20 data at each depth in the matrix of the nearest location were summed up in the time direction. The depth where the summation was the maximal was considered as the focal depth. Then the shear wave speed at this depth was calculated using the RT method described above.

(2) Artificially defined five depths with an uniform distribution in the ROI and calculated shear wave speed at each depth. Then the median of the five speed values was used as the final result.

(3) Averaged all the data at the same time point in the four time-depth displacement matrixes, and used the results to form a time-location displacement matrix for the following shear wave speed calculation based on RT.

B. Type II: RT on time-depth displacement matrix

If the wavefront's time position in the time-depth displacement matrix of four lateral locations can be directly determined, the shear wave propagation time from one location to the other ones can be easily calculated, and then the shear wave speed can be readily estimated. The algorithms based on this conception are described in detail in the following sections.

(1) RT can also be used to obtain the time position of the wavefront in the time-depth displacement matrix. The trajectory corresponding to the maximal summation value is the best approximation of the wavefront. Using the raw displacement data, a coarse position of wavefront was first estimated. Then 20 times cubic spline interpolation was performed in a scope of 10 frames around the time position of wavefront for increasing temporal resolution. At last, more precise wavefront time positions were determined using RT again, and the shear wave speed was calculated according to these positions.

(2) Moreover, we proposed a threshold concept into the Type II(1) algorithm to determine the precise time positions of the wavefronts after the interpolation step. This can reduce the negative influence of the large abnormal values in the displacement signals. Within the scope of interpolation, all the data were summed up in the column (depth) direction and a row (time) vector of summation was obtained. The value equal to 75% of the vector's maximum was defined as the threshold and a time position range where the summation value was greater than this threshold was delineated. The middle point of this range was considered as the precise time position of the wavefront. At last, as the same as the Type II(1) algorithm, shear wave speed values between each two adjacent lateral locations were calculated and averaged as the final result.

Besides the above two types, we also tried to combined them together. First, the coarse time position of the wavefront at each lateral location was determined using RT. Then the depth corresponding to the maximal displacement at this time position was found and thus four different depths were selected. At last, the mean value of the four depth values was selected as the fifth depth and the displacement signals at these five depths were used to calculate the shear wave speed as in the type I(2) algorithm.

C. Reliability and computation speed comparison

Stiffness measurements were performed using a self-developed ARFI system with a self-made 3.5MHz linear array transducer, which was used to both generate and track the shear wave propagation. Experiments were conducted on self-made gelatin phantom and fresh *ex vivo* pork tissue sample. The ROI was identified on the b-mode image with a fixed size of 2×1.5 mm. One data set of RF signals was collected in one ROI with 4 tracking locations, 100 frames per location, and 512 data points per frame. The tissue displacement signals were calculated by an analytic signal based cross-correlation method and were used as the input of the following algorithm tests.

Computation time of each algorithm on one data set was first evaluated using Matlab (The Mathworks, Natick, MA, USA) with its stopwatch timer function. The function can records the internal time at execution of the *tic* command and display the elapsed time with the *toc* command. In the experiment on gelatin phantom, shear wave speeds at eight sites were measured repeatedly, with the ROI moved gradually from a shallow region (20 mm) to a deeper region (80mm). At each site measurement was repeated for 50 times. Then the shear wave speeds were estimated using the six algorithms mentioned above, and the means and standard deviation (SD) of the results were calculated. Finally, the coefficient of variation (CV) defined as the ratio of the SD to the mean was determined to evaluate the reliability of these algorithms. In the experiment on *ex vivo* pork tissue, the depths of the measurement sites were restricted by the thickness of the sample and were set to be 2.5cm, 3cm, 3.5cm and 4cm. Similarly, measurement was repeated for 50 times at each site and the mean, SD and CVs were also calculated.

III. RESULTS

The computation time of the six algorithms is arranged in the order from fast to slow, namely: Type II(2), Type I(3),

Type I(1), Type II(1), Combination and Type I(2), and the time consumption on one data set are 0.53s, 0.60s, 0.61s, 2.80s, 2.93s and 3.01s, respectively. The first three methods are much faster than the other three.

The stiffness of the phantom and the pork tissue is in the same range (the reasonable shear wave speed values are both between 2.5m/s to 3m/s), therefore the CVs obtained on them are comparable. The CVs of all algorithms obtained on phantom are plotted in Figure 1. Trends can be found that the CVs of all algorithms increase at the shallower and deeper measurement positions, and almost all algorithms are most reliable at the middle depth positions (from 4 to 6 cm).

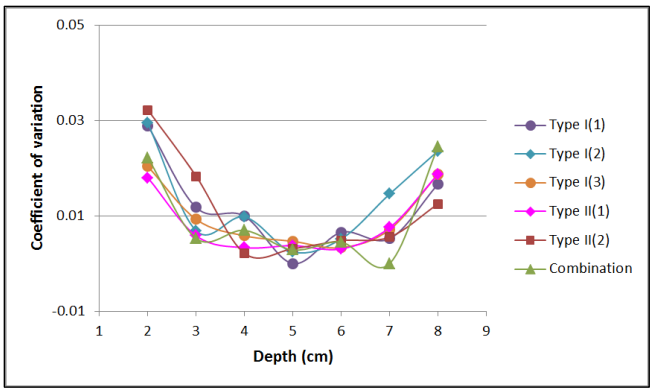

Figure 1. The coefficient of variation (CV) of the shear wave speed estimated by the six algorithms on gelatin phantom.

The CVs of all algorithms obtained on *ex vivo* pork tissue sample are plotted in Figure 2 and their values are much larger than those obtained on phantom. However, similar to the results on phantom, CVs at the deepest measurement position (4cm) are larger than those at the other depths (from 2.5cm to 3.5cm).

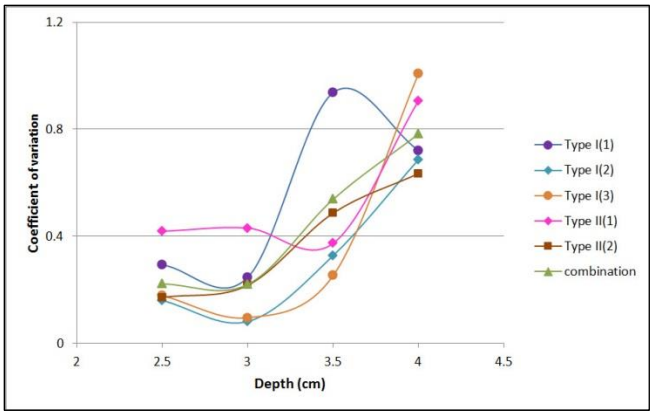

Figure 2. The coefficient of variation (CV) of the shear wave speed estimated by the six algorithms on *ex vivo* pork tissue sample.

IV. Discussion

It has been presented that CV of every algorithm rises at the shallower and deeper positions on both the tissue mimicking phantom and the *ex vivo* pork tissue sample. This phenomenon also appeared in the results of a commercial ultrasound elastography scanner, Aixplorer (SuperSonic Imagine, Aix-en-Provence, France), which can perform quantitative stiffness measurements with similar methods based on acoustic radiation force emission and shear wave speed estimation [24]. It has been proved that this is mainly because of the lower SNR of the displacement signals at these depths. Moreover, the six algorithms have shown their different sensitivities to the changing SNR, especially on the pork tissue sample. CVs obtained on the pork tissue are much larger than those obtained on the phantom at the similar depths. This may be explained by that the elastic property of the phantom are much more uniform than the pork tissue and the SNR of the displacement signals is thus also much higher. Another reason may be the special characteristics of the RF echo signals caused by the complex components and structures of the biological tissue.

The CVs of different algorithms obtained on the phantom are almost similar at the same depth. For Type I algorithms, the SNR of I(2) and I(3) are lower than I(1), especially on the pork tissue sample. This proves that I(2) and I(3) are more effective for improving the reliability. However, the robustness of I(2) and I(3) are different when there are large abnormal values in the displacement signals. In algorithm I(2), the interpolations and RTs are performed at five depths first, then the median speed value is selected from the five results. Therefore its computation amount is much larger than I(1) and I(3). But since the median result will not be easily affected by the abnormal values, the result will be more robust. This can be demonstrated by the CVs obtained on the port tissue at 4 cm depth, which corresponds to the lowest SNR of the displacement signals. And for algorithm I(3), the displacement signals are first averaged, then only one interpolation and RT needs to be performed. Thus the influence of large abnormal values should be much smaller than I(1) but still exists if the abnormal values are extremely large. Nonetheless, the computation amount of I(3) is small and only as about 1/5 as that of I(2).

For Type II algorithms, II(1) calculates twice RTs and interpolations, thus its time consumption is less than I(2) but more than I(3). However, its performance is bad on the pork tissue sample comparing to the other algorithms. The algorithm II(2) also only performs one interpolation and one RT, just like I(3), which makes it the fastest one among the 6 algorithms. And comparing to II(1), using a threshold concept in II(2) can effectively reduce the negative influence caused by the large abnormal values and irregular shape of the wavefronts in the displacement signals, which happened more in the practical data obtained on biological tissue. The good noise immunity of II(2) can be proved by that its CV is the lowest one at the deepest depth on the pork tissue.

And finally, we proposed the combination method of Type I and Type II, trying to use the information of wavefront's time position to determine the depth where the data would be used to calculate the shear wave speed. However, the combination algorithm didn't provide us an enough satisfied result. Both its computation time and reliability are poorer than the other algorithms.

The results obtained on the pork tissue are considered more meaningful than those obtained on the phantom, as the

pork tissue is more similar as that of human being. The reliability of the simplest algorithm I(1) relies on the fortune that not selecting a depth containing large abnormal values. It has been shown that it is not stable enough when the depth increases. When the measurement depth is shallow (from 2.5cm to 3.5cm on the pork tissue), algorithms I(2) and I(3) are better than the others since the averaging and taking median steps of them are more effective when the number and amplitude of the abnormal values are relatively small. However, when the displacement signals become more noisy at the deeper depth (4cm on the pork tissue), algorithm II(2) shows a better performance since the threshold concept can successfully reduce the negative influence caused by the large abnormal values and irregular shape of the wavefronts in the displacement signals. According to the results, we recommend that using the algorithm I(2) or I(3) at the relatively shallower depths, and using the algorithm II(2) at the deeper depths. The detailed conditions for switching the algorithms should be further studied and determined.

There are still some limitations to our study. One is the limited number of measurement depths, especially on the *ex vivo* pork tissue. Despite this, the reason of the appearance of the large abnormal values in the displacement signals should be further affirmed and classified. The more characteristic parameters we extract from these abnormal samples, the more opportunities we have to further improve the algorithms of shear wave speed estimation and the reliability of the repeated measurements in ARFI.

REFERENCES

[1] Chen, S., M. Fatemi, and J.F. Greenleaf, Quantifying elasticity and viscosity from measurement of shear wave speed dispersion. The Journal of the Acoustical Society of America, 2004. 115(6): p. 2781.

[2] Doherty, J.R., et al., Acoustic radiation force elasticity imaging in diagnostic ultrasound. IEEE Trans Ultrason Ferroelectr Freq Control, 2013. 60(4): p. 685-701.

[3] Walker, W.F., Internal deformation of a uniform elastic solid by acoustic radiation force. J Acoust Soc Am, 1999. 105(4): p. 2508-18.

[4] D. Cosgrove, F. Piscaglia, J. Bamber, J. Bojunga, J. M. Correas, O. H. Gilja, et al., "EFSUMB Guidelines and Recommendations on the Clinical Use of Ultrasound Elastography. Part 2: Clinical Applications," Ultraschall in Der Medizin, vol. 34, pp. 238-253, Jun 2013.

[5] Cespedes, I., et al., Elastography: Elasticity Imaging Using Ultrasound with Application to Muscle and Breast In Vivo. Ultrasonic Imaging, 1993. 15(2): p. 73-88.

[6] Pesavento, A., et al., A Time-Efficient and Accurate Strain Estimation Concept for Ultrasonic Elastography Using Iterative Phase Zero Estimation. IEEE Transactions on Ultrasonics, Ferroelectrics, and Frequency Control, 1999. 46(5): p. 1057-1067.

[7] Srinivasan, S. and J. Ophir, A zero-crossing strain estimator for elastography. Ultrasound in Medicine & Biology, 2003. 29(2): p. 227-238.

[8] Eskandari, H., S.E. Salcudean, and R. Rohling, Tissue strain imaging using a wavelet transform-based peak search algorithm. Ieee Transactions on Ultrasonics Ferroelectrics and Frequency Control, 2007. 54(6): p. 1118-1130.

[9] Lindop, J.E., et al., phase-based ultrasonic deformaton estimation. IEEE Transactions on Ultrasonics, Ferroelectrics, and Frequency Control, 2008. 55(1): p. 94-111.

[10] Nightingale, K., S. McAleavey, and G. Trahey, Shear-wave generation using acoustic radiation force: In vivo and ex vivo results. Ultrasound in Medicine and Biology, 2003. 29(12): p. 1715-1723.

[11] Bercoff, J., M. Tanter, and M. Fink, Supersonic shear imaging: a new technique for soft tissue elasticity mapping. IEEE Trans Ultrason Ferroelectr Freq Control, 2004. 51(4): p. 396-409.

[12] Palmeri, M.L., et al., Ultrasonic tracking of acoustic radiation force-induced displacements in homogeneous media. IEEE Trans Ultrason Ferroelectr Freq Control, 2006. 53(7): p. 1300-13.

[13] Pinton, G.F., J.J. Dahl, and G.E. Trahey, Rapid tracking of small displacements with ultrasound. IEEE Trans Ultrason Ferroelectr Freq Control, 2006. 53(6): p. 1103-17.

[14] Oliphant, T.E., et al., Complex-valued stiffness reconstruction for magnetic resonance elastography by algebraic inversion of the differential equation. Magn Reson Med, 2001. 45(2): p. 299-310.

[15] Sandrin, L., et al., Shear modulus imaging with 2-D transient elastography. IEEE Trans Ultrason Ferroelectr Freq Control, 2002. 49(4): p. 426-35.

[16] Sinkus, R., et al., Viscoelastic shear properties of in vivo breast lesions measured by MR elastography. Magnetic Resonance Imaging, 2005. 23(2): p. 159-165.

[17] Sandrin, L., et al., Transient elastography: a new noninvasive method for assessment of hepatic fibrosis. Ultrasound in Medicine & Biology, 2003. 29(12): p. 1705-1713.

[18] McLaughlin, J. and D. Renzi, Shear wave speed recovery in transient elastography and supersonic imaging using propagating fronts. Inverse Problems, 2006. 22(2): p. 681-706.

[19] McLaughlin, J. and D. Renzi, Using level set based inversion of arrival times to recover shear wave speed in transient elastography and supersonic imaging. Inverse Problems, 2006. 22(2): p. 707-725.

[20] Palmeri, M.L., et al., Quantifying hepatic shear modulus in vivo using acoustic radiation force. Ultrasound Med Biol, 2008. 34(4): p. 546-58.

[21] Tanter, M., et al., Quantitative Assessment of Breast Lesion Viscoelasticity: Initial Clinical Results Using Supersonic Shear Imaging. Ultrasound in Medicine & Biology, 2008. 34(9): p. 1373-1386.

[22] Rouze, N.C., et al., Robust Estimation of Time-of-Flight Shear Wave Speed Using a Radon Sum Transformation. Ieee Transactions on Ultrasonics Ferroelectrics and Frequency Control, 2010. 57(12): p. 2662-2670.

[23] C. Simon, P. VanBaren, and E. S. Ebbini, "Two-dimensional temperature estimation using diagnostic ultrasound," IEEE Trans. Ultrasonics ferroelectrics and frequency control, vol. 45, pp. 1088-1099, Jul 1998.

[24] CZ. Wang, J. Zheng, ZP. Huang,Y. Xiao, D. Song, J. Zeng, HR. Zheng and RQ. Zheng, " Influence of Measurement Depth on the Stiffness Assessment of Healthy Liver with Real-time Shear Wave Elastography," Ultrasound in Medicine and Biology, vol. 40, no. 3, pp. 461–469, 2014